


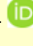


# Simulation of landslide run-out by considering frictional heating and thermal pressurization

**LIU Wei**<sup>1,2</sup>  <http://orcid.org/0000-0001-6336-4387>; e-mail: sponlol@163.com

**HE Si-ming**<sup>1,2,3\*</sup>  <http://orcid.org/0000-0002-7372-8938>;  e-mail: hsm@imde.ac.cn

**HE Zi-lu**<sup>4</sup>  <http://orcid.org/0000-0003-4519-2475>; e-mail: xiaotonlele@sohu.com

\*Corresponding author

*1 Key Laboratory of Mountain Hazards and Surface Process, Chinese Academy of Science, Chengdu 610041, China*

*2 Institute of Mountain Hazards and Environment, Chinese Academy of Sciences, Chengdu 610041, China*

*3 CAS Center for Excellence in Tibetan Plateau Earth Sciences, Beijing 10010, China*

*4 Department of Applied Mechanics and Engineering, Southwest Jiaotong University, Chengdu 611756, China*

**Citation:** Liu W, He SM, He ZL (2019) Simulation of landslide run-out by considering frictional heating and thermal pressurization. *Journal of Mountain Science* 16(1). <https://doi.org/10.1007/s11629-018-5012-4>

© Science Press, Institute of Mountain Hazards and Environment, CAS and Springer-Verlag GmbH Germany, part of Springer Nature 2019

**Abstract:** Some of the remarkable characteristics of natural landslides, such as surprisingly long travel distances and high velocities, have been attributed to the mechanisms of frictional heating and thermal pressurization. In this work, this mechanism is combined with a depth-averaged model to simulate the long runout of landslides in the condition of deformation. Some important factors that influence frictional heating and thermal pressurization within the shear zone are further considered, including velocity profile and pressurization coefficient. In order to solve the coupled equations, a combined computational method based on the finite volume method and quadratic upwind interpolation for convective kinematics scheme is proposed. Several numerical tests are performed to demonstrate the feasibility of the computational scheme, the influence of thermal pressurization on landslide run-out, and the potential of the model to simulate an actual landslide.

**Keywords:** Landslide; Frictional heating; Thermal pressurization; Numerical simulation

**Received:** 09 May 2018

**Revised:** 26 September 2018

**Accepted:** 08 October 2018

## Introduction

Natural landslides can have large travel distances and high velocities, causing widespread damage. Recent examples of such landslides include the 1963 Vaiont landslide in Italy (Ferri et al. 2011), the 2009 Hsiaolin landslide in China's Taiwan (Kuo et al. 2011), and the Daguangbao landslide that was induced by the Wenchuan earthquake in China's Sichuan Province (Huang and Fan 2013). However, the physical phenomena underlying natural landslides are still not entirely understood.

For explaining the higher mobility mechanism of landslides, several theories have been proposed, including dynamic fragmentation (Rait et al. 2012; Mazzanti and De Blasio 2013), the air-cushion effect (Shreve 1968; Erismann 1979), entrainment (Pirulli and Pastor 2012; Iverson et al. 2011), fluidization (Huang et al. 2011; Pastor et al. 2015), and lubrication (Cleary and Campbell 1993; De Blasio 2011). In recent decades, as one of the key possible explanations for the unusually long run-out of some natural landslides, frictional heating of

the shear zone has long been considered (Habib 1975; Voight and Faust 1982; Vardoulakis 2002; Goren and Aharonov 2009; Cecinato and Zervos 2012; Hu et al. 2018). Pore pressure at the shear zone was enhanced by thermal pressurization that caused by frictional heating, which could induce rapid frictional strength loss and thus increase the mobility of the landslide. Based on field investigation, Voight and Faust (1982) first proposed this mechanism, and pointed out that it could be influenced by the friction coefficient, porosity, slide displacement, slip zone thickness and compressibility. Further, Vardoulakis (2000) presented a thermo-poro-mechanical model for describing the evolution of temperature and pore-fluid pressure within the slip plane of landslide. More recently, to explain the phenomenon that the apparent friction coefficient decreases with increasing slide volume, Goren and Aharonov (2007) proposed a thermo-poro-elastic mechanism operating at the base of landslides. The relevant parameters that control the stability of the sliding process were also investigated by Goren and Aharonov (2009), such as sliding thickness and permeability. However, as a most important parameter that influences thermal pressurization significantly, the value of the pressurization coefficient is always treated as a constant in these models. Its variation during landslide run-out is neglected, yet it may significantly influence the evolution of the pore pressure.

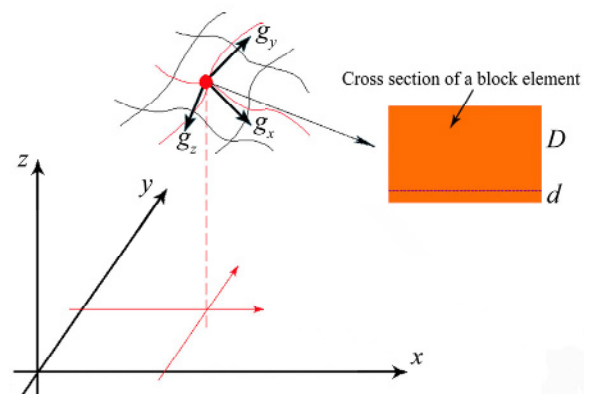
In past years, thermal pressurization due to frictional heating has been studied in a number of different contexts (Sultan et al. 2002; Wibberley and Shimamoto 2005). Noda and Shimamoto (2005) analysed the thermal pressurization process by modelling the Hanaore fault zone in Japan, and found that this process influenced the heat production heat rate effectively. Ghabezloo and Sulem (2009) studied the phenomenon of thermal pressurization based on the undrained heating test, and further analysed the relationships between stress, thermal pressurization and temperature. A high-velocity experiment was performed by Ferri et al. (2010) to provide the evidence of thermal pressurization. By adopting a more general constitutive assumption for the soil, a new thermo-mechanical model was developed by Cecinato et al. (2012). In these studies, the pressurization coefficient is determined by other relevant material

parameters and state variables, rather than consider it an independent parameter. Nevertheless, the objects of these studies mainly focused on fault slip or landslides with rigid body, the study of landslide run-out by taking into account the condition of deformation is still lack.

In this paper, a deformation model of landslide run-out based on frictional heating and thermal pressurization is presented. This model considers heat production and diffusion, pore-fluid pressure generation and dissipation, and temperature dependence of the pressurization coefficient at the shear zone. Moreover, some important factors that influence the frictional heating are investigated. The well-documented large-scale landslide of Jiufengershan is also analysed as an example.

## 1 Model Equations

A schematic of a landslide moving down a curved surface is shown in Figure 1. The model employs a fixed Cartesian coordinate system  $(x, y, z)$  where the  $z$ -axis is parallel to the direction of the gravitational acceleration. The symbols  $g_x$ ,  $g_y$  and  $g_z$  represent the components of the gravitational acceleration in the surface-induced down-slope, cross-slope and normal directions, respectively (Fischer et al. 2012). A cross section of the block element shows that the evolutions of temperature, pore-fluid pressure and soil properties are concentrated along a thin shear zone with



**Figure 1** Sketch of a slide of the landslide block element in a fixed Cartesian coordinate system  $(x, y, z)$ , and  $z$  points in the direction of the gravitational acceleration. Orange area represents the cross section of a block element of landslide.

thickness  $d$  at the base of the mass. Values differing in orders of magnitude, ranging from  $10^{-4}$  to 1 m are offered for the shear zone thickness that is much less than the total height  $D$  of the mass (Vardoulakis 2000; Rice 2006; Goren and Aharonov 2007).

With the introduced coordinate system, a widely used hyperbolic system of conservation laws derived from the depth-averaged equations is applied to simulate the landslide run-out by neglecting the changes in the vertical motion characteristics of the landslide (Savage and Hutter 1989; Pitman et al. 2003; Domnik et al. 2013; George and Iverson 2014):

$$\frac{\partial h}{\partial t} + \frac{\partial hu}{\partial x} + \frac{\partial hv}{\partial y} = 0 \quad (1)$$

$$\frac{\partial hu}{\partial t} + \frac{\partial}{\partial x} \left( hu^2 + \frac{1}{2} k_x g_x h^2 \right) + \frac{\partial huv}{\partial y} \quad (2)$$

$$= g_x h - \frac{u}{|\mathbf{u}|} \mu \left( g_z h (1-r) - \frac{p}{\rho} \right)$$

$$\frac{\partial hv}{\partial t} + \frac{\partial huv}{\partial x} + \frac{\partial}{\partial y} \left( hv^2 + \frac{1}{2} k_y g_y h^2 \right) \quad (3)$$

$$= g_y h - \frac{v}{|\mathbf{u}|} \mu \left( g_z h (1-r) - \frac{p}{\rho} \right)$$

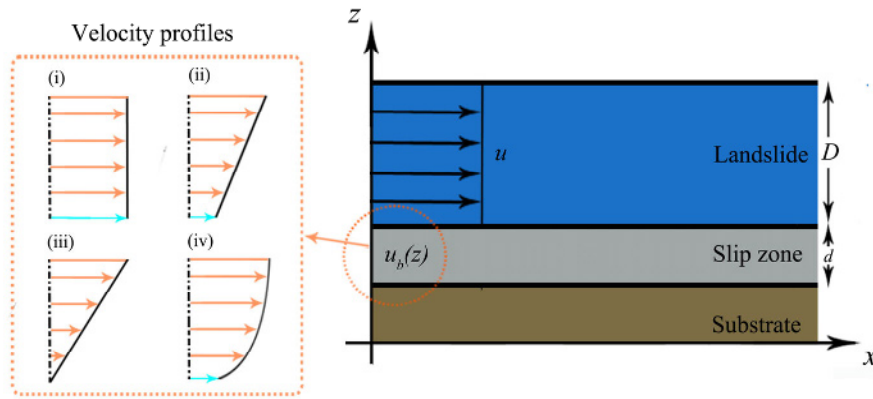
where  $t$  is the time;  $h$  is the landslide height;  $\mathbf{u} = (u, v)$  is the Cartesian velocity;  $\rho = (1-n)\rho_f + n\rho_s$  is the density of the landslide body, where  $\rho_s$  is the solid density,  $\rho_f$  is the fluid density and  $n = e/(1+e)$  is the porosity of landslide body;  $e$  is the void ratio;  $r = \rho_f/\rho$  is the density ratio, which indicates that the mass is assumed to be fully water saturated;  $\mu = \tan\delta$  is the friction coefficient; and  $\delta$  is the basal friction angle;  $\mathbf{k} = (k_x, k_y)$  is the lateral earth pressure coefficient, and a simple idealisations  $k_x = 1$  and  $k_y = 1$  are employed (Gray et al. 2003; Iverson and George 2016);  $p$  is the excess pore pressure induced by friction heating. According to Goren and Aharonov 2007, the value of  $p$  that locates at the middle of the shear zone is adopted. Eq. 1 represents the mass conservation for the landslide. Eqs. 2-3 represent the momentum conservation equation for unit volume of the landslide. The first two terms on the right hand side of Eqs. 2-3 indicate the gravity force and the frictional resistance in  $x$  and  $y$  directions, respectively. A Coulomb friction sliding law is adopted to describe the frictional resistance, which expresses the fact that the magnitude of the basal shear stress equals

the normal basal pressure multiplied by a friction coefficient. It means that the larger the normal stress exists (the larger the volume of siding is), the more heat is created due to frictional heating. Then, the temperature at the shear zone could raise fast and cause pore water pressure to increase more remarkable. The friction is reduced by the rise in pore water pressure, and a greater sliding distance of landslide is produced.

During the sliding process, the temperature within the shear zone changes with frictional heating, which further influences the behaviour of a landslide body by changing soil properties such as volumetric strains and thermal softening (Cui et al. 2000; Tomac and Gutierrez 2015). According to Goren and Aharonov (2007), the evolution equation of temperature within the shear zone can be derived from energy conservation considerations:

$$\rho c \frac{\partial \theta}{\partial t} = \frac{\partial}{\partial z} k_\theta \frac{\partial \theta}{\partial z} + \tau(p) \frac{\partial |\mathbf{u}|}{\partial z} \quad (4)$$

where  $\theta$  is the temperature;  $c = (1-n)c_f + nc_s$  is the specific heat of the landslide, where  $c_f$  and  $c_s$  are the specific heat of the fluid and solid, respectively;  $k_\theta$  is the thermal conductivity of the saturated rock in  $\text{W m}^{-1} \text{ }^\circ\text{C}^{-1}$ ;  $\tau(p)$  is the shear stress. Here, the landslide body is assumed to be saturated so that the fluid pressure is initially hydrostatic, and the shear stress  $\tau(p) = \mu\rho(g_{zz} - rg_{zz} - p/\rho)$ .  $\partial|\mathbf{u}|/\partial z$  represents the velocity gradient along the shear zone, and is an important factor that influences frictional heating (Mase and Smith 1984; Kilgore et al. 1993). Figure 2 shows a schematic diagram of the vertical velocity profile of landslide. Actually, the velocity profile within the shear zone may changes as the velocity of the mass above changes, however, which is too complex to be considered. Thus, some particular velocity profiles investigated by Johnson et al. (2012) are chosen and shown in Figure 2. Generally, for slope engineering purposes, the rheological behavior (e.g. viscoplasticity) will lead to choose velocity profile (i) if the shear zone is composed of homogeneous soft materials. Instead, velocity profile (iii) and (iv) might be more appropriate if the shear zone is made up with competent geological formations which indicate that corresponding material mechanical behaviour is stiffer. The first and second terms on the right hand side of Eq. 4 express heat conduction and



**Figure 2** Schematic diagram of velocity profile  $u_b(z)$  within the slip zone, depth-averaged velocity of landslide body  $u$  and some commonly velocity profiles (i, ii, iii and iv) along the  $z$  direction. (i) illustrates plug flow, (ii) illustrates the combination of shear and basal slip (Johnson et al. 2012) and (iii) illustrates simple shear. In addition, (iv) represents the flow with undetermined velocity profile.

heat production at the shear zone by frictional heating, respectively. Moreover, a comprehensive form of Eq. 4 for describing temperature evolution should also include the heat advection. However, compare to sliding time of landslides, the time scale of this term is too large to changes the overall travel distance of the landslides significantly (Goren and Aharonov 2007). Thus, this term is neglected in this study, and the temperature is considered to be influenced solely by frictional heating within the shear zone.

For excess pore-fluid pressures equation, it should be complied with the Darcy’s law and conservation of mass (Cecinato et al. 2011). By considering the influences of temperature variation, the time evolution of excess pore pressure can be described as:

$$\frac{\partial p}{\partial t} = \frac{\partial}{\partial z} \left( B_v \frac{\partial p}{\partial z} \right) + \Lambda \frac{\partial \theta}{\partial t} \quad (5)$$

where  $\Lambda$  is the pressurization coefficient, and can be influenced by temperature;  $B_v$  is the consolidation coefficient, which can be expressed as:

$$B_v = \frac{k_c}{g \rho_f S_c} \quad (6)$$

where  $k_c$  is Darcy’s permeability coefficient;  $S_c$  is the soil compressibility and can be written as:

$$S_c = \left( \frac{e}{1+e} \right) r_f + \frac{\kappa(1+\nu)}{3p_0(1-\nu)(1+e)} \quad (7)$$

where  $r_f$  is the fluid compressibility;  $\kappa$  is the

(dimensionless) slope of the unloading–reloading line of the soil;  $p_0$  is the mean effective stress under initial condition;  $\nu$  is the Poisson ratio of the soil. As suggested by Hu and McSaveney (2018), high-pressure live steam and carbon dioxide could be produced by water vaporization and mineral changes if the temperature at the base of landslide reaches to a high enough level, which could further decrease the frictional resistance from the sliding

surface. Evidences of these phenomena have been found on both high-speed rotary shear experiments and field observations (Hu et al. 2018). However, due to the complex mechanisms within the shear zone during the sliding process of a landslide, these special phenomena are not considered in this study.

Recently, the phenomena of plastic contraction of soil upon heating, which influences the soil’s volumetric behaviour, has been recognized by many authors (Vardoulakis 2002; Sulem et al. 2007; Ghabezloo and Sulem 2009). The variations of plastic contraction and soil’s volumetric behaviour further have an effect on  $\Lambda$ , and further influences thermal pressurization. Here, a relationship between  $\Lambda$ , plastic contraction and soil compressibility, proposed by Vardoulakis (2002) and further modified by Cecinato et al. (2011), has been adopted as:

$$\Lambda = - \frac{\alpha_c^p(\theta)}{S_c} \quad (8)$$

where  $\alpha_c^p(\theta)$  is the thermo-plastic contraction coefficient and expressed as:

$$\alpha_c^p(\theta) = \frac{\lambda - \kappa}{\lambda} \left\{ \frac{\gamma \kappa}{(1+e) \{1 - \log(\theta/\theta_{ref})\}} \theta - 2\beta_s \right\} \quad (9)$$

where  $\lambda$  is the (dimensionless) slope of the normal-compression line of the soil;  $\theta_{ref}$  is the reference value of temperature; and  $\beta_s = (1-n) \alpha_s + n \alpha_f$  is the thermoelastic expansion coefficient, where  $\alpha_s$  is the coefficient of thermal expansion of particles and  $\alpha_f$

is the coefficient of thermal expansion of water (Laloui et al. 2005). The first and second terms on the right hand side of Eq. 5 express pore fluid pressure dissipation and pore fluid pressure production caused by temperature evaluation at the shear zone, respectively.

## 2 Computational Scheme

Here, a finite volume discretization of a computational domain in the  $x$ - $y$ - $z$  directions is shown in Figure 3. However, it could be found that the variables of landslide evolve in different directions which should be computed simultaneously within a time step. Based this case, we coupled the finite volume method and Quadratic Upwind Interpolation for Convective Kinematics (QUICK) scheme for solving the model equations. Figure 4 illustrates the steps of the presented numerical scheme by using a flow chart. Firstly, we used the finite volume method to solve Eqs. 1-3 to obtain the next time state of variables ( $h$ ,  $u$ ,  $v$ ) in the  $x$  and  $y$  directions. Then, we used the QUICK scheme to obtain the next time state variables ( $\theta$ ,  $p$ ) to solve Eqs. 4-5 in the  $z$  direction. In a feedback cycle, all the variables are updated and used for the next iteration. More details are given below

Eqs. 1-3 represent a shallow flow problem which has been solved by many researchers by using finite volume method (Soares-Frazão and Zech 2011; LeFloch and Thanh 2011; Balsara 2012; Ambroso et al. 2012), and more details can be found in Liang and Borthwick (2009). After obtaining the velocity and height of the landslide, the temperature and pore water pressure equations can be further solved. Here, a modified QUICK scheme is adopted to solve the temperature and pore pressure equations in the vertical direction as an unsteady convection-diffusion problem (Hayase et al. 1992; Leonard 1995). For example, the interface fluxes of  $\theta$  are calculated as

$$\begin{cases} \theta_u = \theta_i + \frac{1}{8}(3\theta_{i+1} - 2\theta_i - \theta_{i-1}) \\ \theta_b = \theta_{i-1} + \frac{1}{8}(3\theta_i - 2\theta_{i-1} - \theta_{i-2}) \end{cases}; \quad (10)$$

where  $\theta_u$  and  $\theta_b$  are the fluxes through the upper and bottom cell interfaces in the  $z$  direction, respectively. It should be noted that the value of

the time step  $\Delta t$  depends on the calculation stability of the finite volume scheme. To ensure the stability of the calculation, a fully implicit scheme that is unconditionally stable is applied to discretize these equations. Thus, the equation for the evolution of temperature can be rewritten as:

$$a_i \theta_i = a_b \theta_b + a_u \theta_u + a_i^0 \theta_i^0 + s_u \quad (11)$$

in which

$$\begin{aligned} a_b &= \frac{\Delta t k_\theta}{\Delta z^2 \rho c}, \quad a_u = \frac{\Delta t k_\theta}{\Delta z^2 \rho c}, \quad a_i^0 = 1, \\ s_u &= \frac{1}{8} a_b (3\theta_i^0 - \theta_{i-1}^0) + \frac{1}{8} a_b (\theta_{i-1}^0 + 2\theta_i^0 - 3\theta_{i+1}^0) \\ &+ \tau(p) \frac{\partial |u|}{\partial z}, \quad a_i = a_i^0 + a_b + a_u \end{aligned} \quad (12)$$

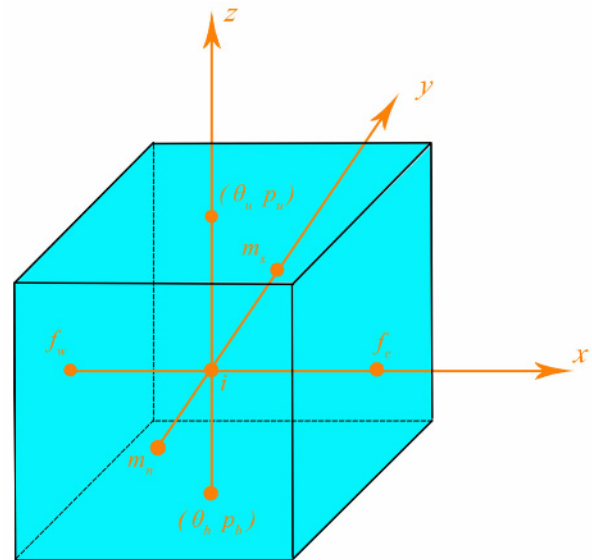


Figure 3 Finite volume discretization of a three-dimensional domain in the  $x$ - $y$ - $z$  directions with a staggered-grid system.

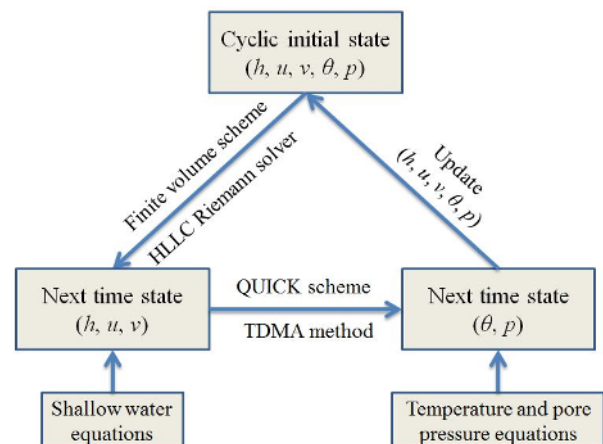


Figure 4 Flow chart of steps of the method.

where  $\Delta z$  is the side length of a grid cell in the  $z$  direction. After the discretization, Eq. 11 becomes a tri-diagonal matrix equation. Thus, the Tri-diagonal matrix algorithm (TDMA) method is adopted to solve the problem (He et al. 2015). Similarly, this procedure is also used to derive an equation for the excess pore pressure.

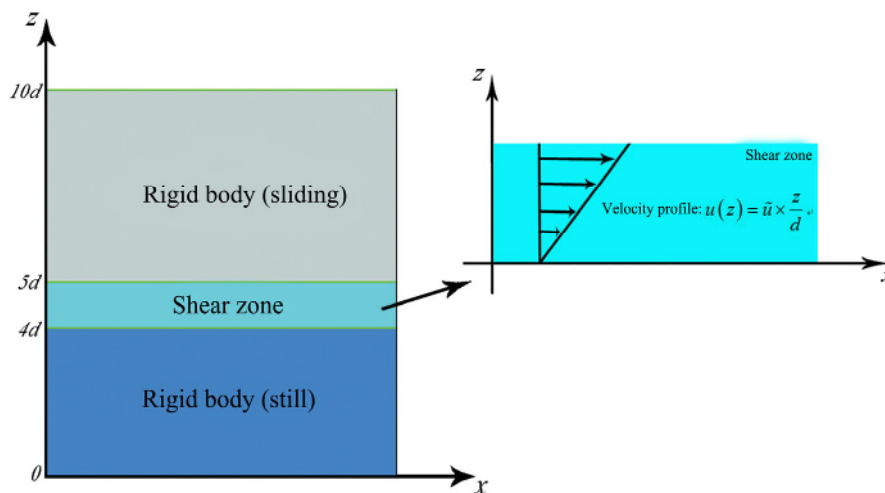
### 3 Results and Discussions

In this section, three numerical experiments were performed to verify the influences of some important factors on thermo-plastic mechanics and the feasibility of the presented model. In these computational experiments, the Courant number is set as  $cfl = 0.7$ , and the gravitational acceleration is  $g = 9.8 \text{ m s}^{-2}$ .

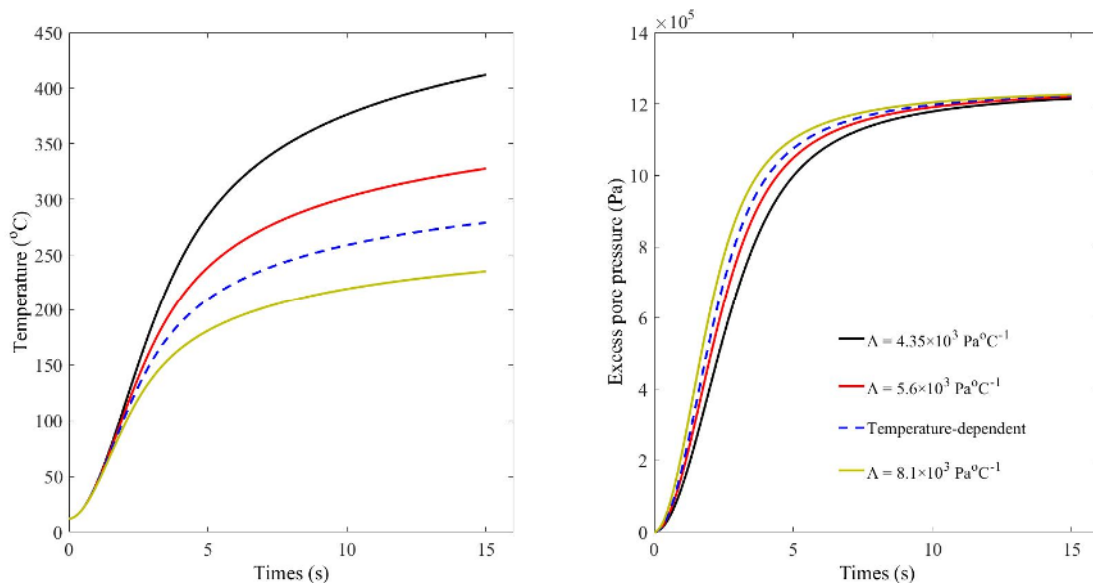
#### 3.1 Analysis of variation of the thermal pressurization coefficient

The long run out of a large-scale landslide always has a low frictional resistance that is due to the frictional heating-induced generation of excess pore pressure at the shear zone. The key mechanism governing the generation of excess pore pressure is thermal pressurization, which is mainly reflected in the value of the pressurization coefficient  $\Lambda$  (Andrews 2002; Wibberley and Shimamoto 2005; Noda and Shimamoto 2005). Generally, the value of the pressurization coefficient is influenced by temperature at the

shear zone, and it further affects the generation of excess pore pressure. In this subsection, this feature is discussed by simulating a simple sliding performed by Cecinato et al. (2011) (Figure 5). The soil layer with a total thickness  $10d$  is divided into three sections: the still lower layer, an upper layer that moves at velocity  $\mathbf{u}$ , and the shear zone with a linear decreasing velocity profile. The relevant parameters are the same as those in Cecinato et al. (2011) except that the friction angle used for the simulation remains constant and the slide thickness  $D = 100 \text{ m}$ . Simulation is carried out for a total time of 15 s. With these parameters, the initial value of the pressurization coefficient is  $5.6 \times 10^3 \text{ Pa } ^\circ\text{C}^{-1}$ . Thus, three values of the pressurization coefficient are applied to the cases that with a constant pressurization coefficient,  $\Lambda = 4.35 \times 10^3, 5.6 \times 10^3$  and  $8.1 \times 10^3 \text{ Pa } ^\circ\text{C}^{-1}$ . Figure 6 shows the evolutions of temperature and excess pore pressure at the middle of the shear zone under different conditions of pressurization coefficient. They indicate that a temperature with a large/small constant pressurization coefficient increases slower/faster than a temperature with a temperature-dependent pressurization coefficient. For excess pore pressure, it increases with the increase of pressurization coefficient, but the variation is small compared with that of temperature. This phenomenon can be considered that the thermal pressurization is enhanced by the temperature increasing, further lead to a greater excess pore pressure at the shear zone which reduces the frictional resistance. In turn, the heat



**Figure 5** The shear zone is a strain localization zone of thickness  $d$ , embedded in an otherwise homogeneous soil layer of total thickness  $10d$ . The soil below the shear zone is still, while the soil at the top of the shear zone moves at velocity  $\mathbf{u}$ . In the shear zone, the assumed velocity profile is linear.



**Figure 6** The curves of temperature and pore pressure with time at the middle of shear zone under different conditions of pressurization coefficient.

produced by friction becomes small due to small frictional resistance, which slows down the increase of temperature.

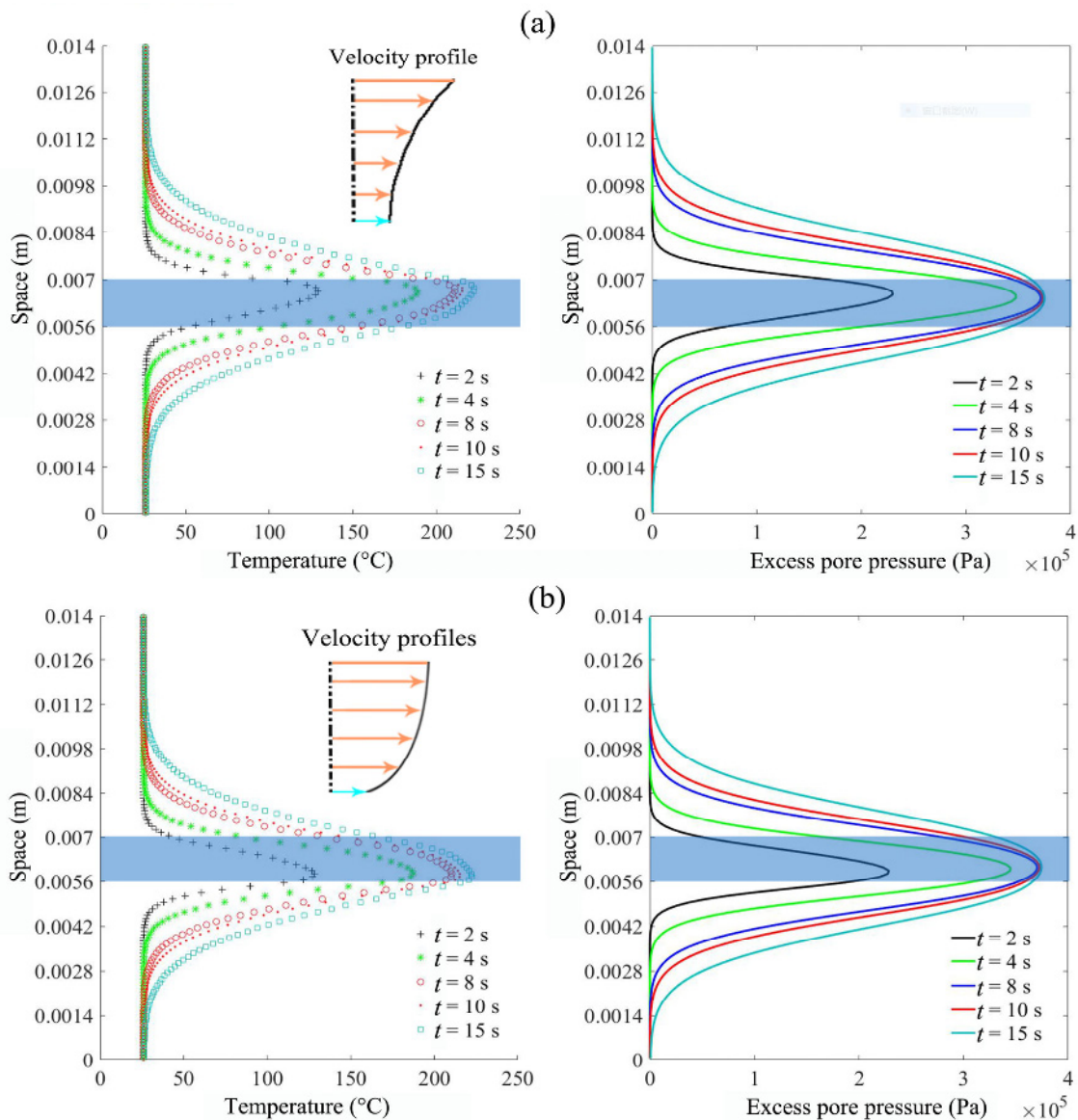
### 3.2 Analysis of variation of the velocity profile within the shear zone

In this section, the influences of different velocity profiles that within the shear zone on heat production and diffusion, as well as pore pressure evolution, are further discussed. The setup of numerical experiment and relevant parameters are also same with [Cecinato et al. \(2011\)](#). However, it is difficult to determine the velocity profile within the shear zone of a real landslide case, and the choice of a realistic velocity profile will be driven by several considerations. Thus, four commonly velocity profiles investigated by [Johnson et al. \(2012\)](#) are used for simulation which is carried out for a total time window of 15 s. The resulting temperature and excess pore pressure with different velocity profiles are shown in [Figure 7](#). All of them indicate that the sliding block accelerates due to gravity and produces friction heating at the shear zone. The temperature in the shear zone rises and causes pore water pressure increase due to frictional heating. The friction is reduced by the rise in excess pore pressure and a greater slope displacement distance is observed. However, some differences in temperature and excess pore pressure are observed depending on the studied

velocity profiles. By comparing [Figure 7\(a\)](#), [7\(b\)](#) and [7\(c\)](#), it can be found that the maximum values of the temperature and excess pore pressure are positioned in the area where the velocity gradient difference (i.e. discontinuity in velocity profile) is the largest. Moreover, with larger velocity gradients, the evolution of the temperature and excess pore pressure become faster as shown by comparing [Figure 7\(b\)](#), [7\(c\)](#) and [7\(d\)](#). These results indicate that more frictional heat can be generated with a larger velocity gradient. Therefore, temperature can rise faster, which lead to the effect of thermal pressurization more obvious. Based on numerical results, it can be deduced that the effect of velocity profiles within the slip zone is of the utmost importance for a proper analysis the sliding process. With different velocity profile in the shear zone, the effects of frictional heating and thermal pressurization on landslide run-out could differ bigger.

### 3.3 Numerical simulation of a block sliding down with different thickness

In order to verify the ability of the presented model capture the evolutions of temperature and excess pore pressure during the landslide motion process, a numerical test from [Goren and Aharonov \(2007\)](#) is performed. As shown in [Figure 8](#), a block element of thickness  $D$  drops from a height of  $H = 5$  m along a slope titled with the angle



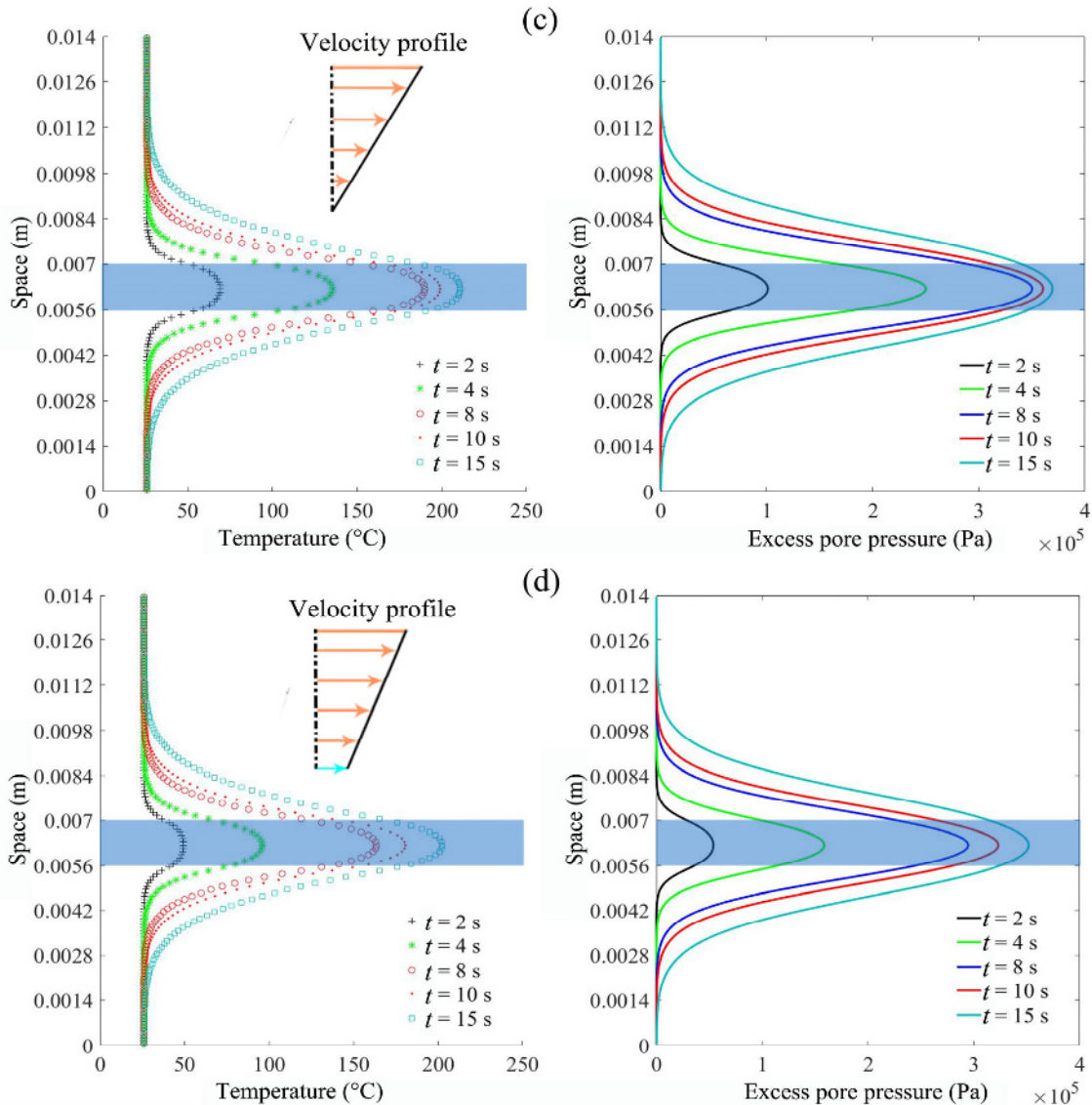
**Figure 7** Temperature and pore pressure isochrones within the shear zone (blue area) and its surroundings, for the different velocity profiles.(-To be continued-)

$\delta$ . It is assumed that the sliding block is an intact body and the deformation is concentrated along a thin shear zone with thickness  $d$  at the base of the slide. The parameters used for simulation are same as Goren and Aharonov (2007). Here, a symbol  $\omega$  is set as  $\omega = p/\rho g D$ . The numerical results in Figure 9 show that the block accelerates due to gravity and produces friction heating at the shear zone, further lead to the change of temperature and excess pore pressure. The temperature at the shear zone rises and causes pore water pressure to increase due to frictional heating. The friction is reduced by the rise in excess pore pressure, and a greater distance is produced. As the block

continues sliding on the plane, it starts to decelerate because gravity does not drive continued sliding and the frictional resistance increases immediately. The lower velocities result in lower rates of heat production, and after some delayed time pore pressure decreases. Figure 9 also reflects that the block with larger thickness has a longer travel distance. It can be considered that more friction heating is produced with a larger shear stress, which causes larger pore water pressure to increase. The tendency of these variables to change can be captured by the proposed numerical method and agrees well with results described in Goren and Aharonov (2007).



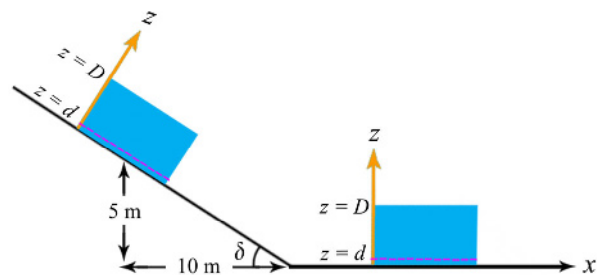
(-Continued-)



**Figure 7** Temperature and pore pressure isochrones within the shear zone (blue area) and its surroundings, for the different velocity profiles.

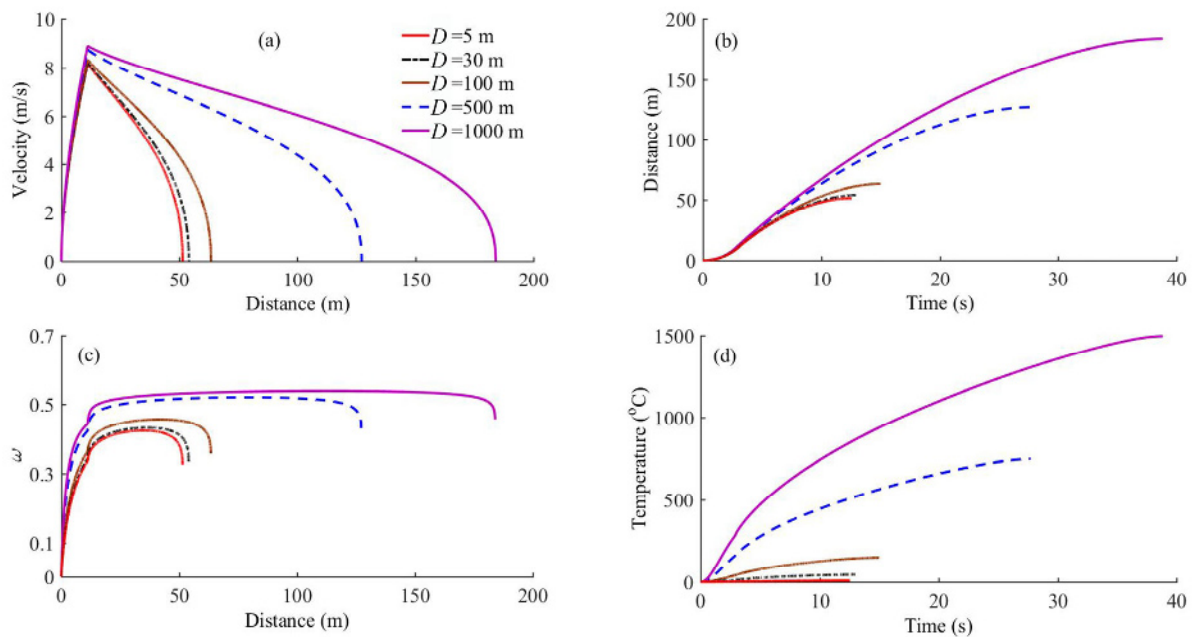
### 3.4 Numerical example: the Jiufengershan landslide

Herein, the current numerical model is applied to simulate the movement of the Jiufengershan landslide. There were four major reasons for choosing this particular landslide: first, it had a planar slip surface and a relatively long sliding distance; second, the slip surface existed bedding-parallel clay seams that with clear slickensides and dip-slip striations throughout the slope (Wang et al. 2003; Dong et al. 2009); third, there was direct field evidence (e.g. the presence of pseudotachylite) (Chang et al. 2005), which implies that the rock



**Figure 8** Model geometry. A block element slides down a slope tilted with the angle  $\delta$ . The block thickness is  $D$  and the shear zone thickness is  $d$ .

must have been heated to temperature in excess of  $1100^{\circ}\text{C}$  that presumably occurred at locations of the slip plane; fourth, the water table was located



**Figure 9** (a) Velocity and (c) pore water pressure evolution with sliding distance; (b) sliding distance and (d) temperature evolution with sliding duration.

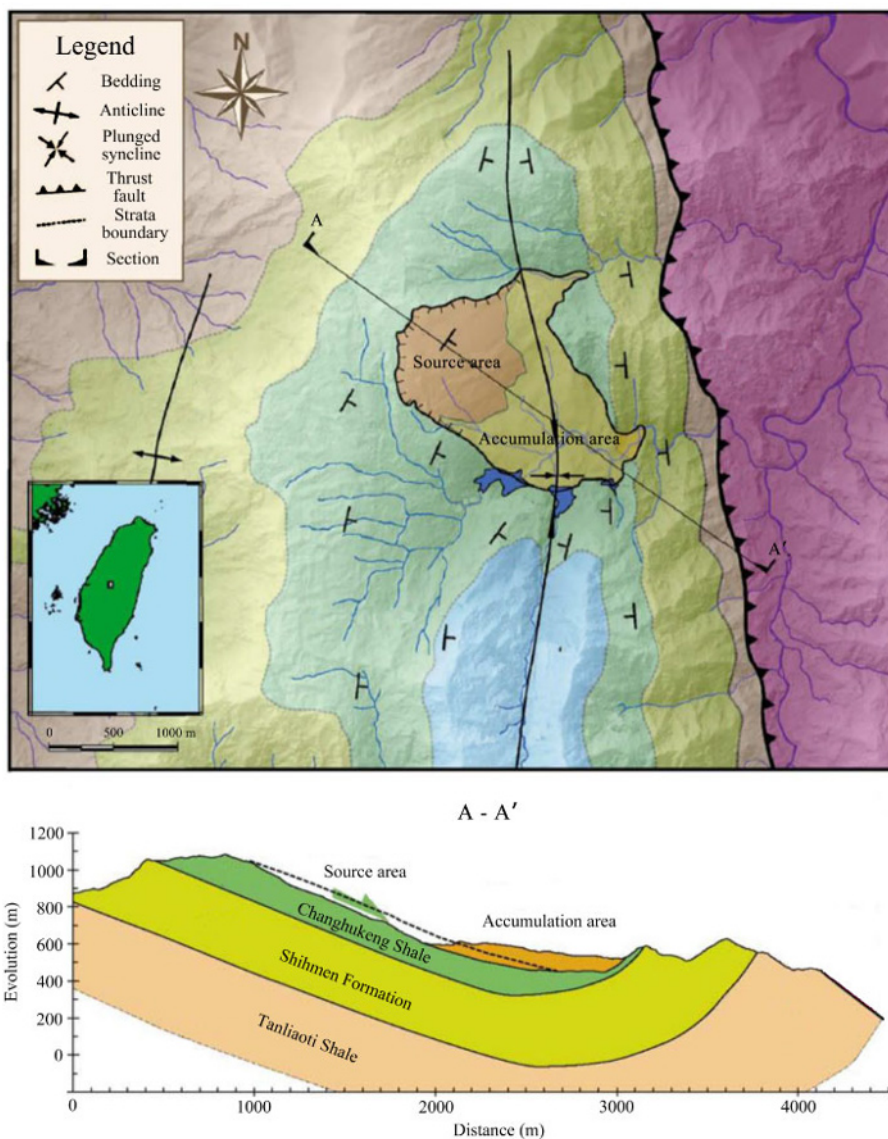
well above the sliding surface according to the water seepage observed on the sliding plane, which was favor of generating excess pore water pressure in shear zone, and the pre-existing fractures and joints filled with mud (Chang and Taboada 2009). Then, it is reasonably expect similar sliding-induced heat production and pore-water pressurization to have taken place within the clay as well. It should be note that the presented model cannot simulate the co-seismic inertial displacements that is a typical behaviour of landslide at early stage. Since the depth-averaged theory is applied to the model equations, the changes of motion characteristics of the landslide in vertical direction also cannot be simulated.

On 21 September 1999, the Jiufengershan landslide that triggered by the Chi-Chi earthquake occurred in Taiwan, causing 39 fatalities. It initially slid along the bedding plane as a translational rock slide, and further transformed into an avalanche as the mass velocity increased and the shear strength at the slip surface decreased (Chang et al. 2009). The Jiufengershan landslide had a total displacement of approximately 1000 m and the slide area was about 75 ha (see Figure 10) (Tang et al. 2012). The sliding mass was chiefly composed of muddy sandstone and dark gray shale. The terrain data used in the simulation are generated from the digital elevation model (DEM) data that has a

spatial resolution of  $5\text{ m}\times 5\text{ m}$ . These DEM data came from the Taiwan Forestry Bureau, and was obtained by remote sensing techniques in 1998 and 2007, respectively. In this case, we take the topography difference before and after the landslide at the source area as the initial source of landslide. The total initial volume in the computation is  $3.5\times 10^7\text{ m}^3$ . It is suggest that the slip occurred at the interface between rock and the clay seams according to the filed observation (Wang et al. 2003), and therefore assumed that deformation was localized within the clay layer. Since the saturated clay can be considered as a soft material (Miura et al. 2001; Abuel-Naga et al. 2007), velocity profile (a) within the shear zone is adopted, which indicates that the closer to the bedrock the smaller the velocity gradient. However, the information about the geotechnical properties of the clay that existed in the Jiufengershan landslide is not available. Thus, the existing mid-range values of clay are used for describing the clay properties. According to Vardoulakis (2000) and Cecinato and Zervos (2012), the differences of thermomechanical properties between different types of soil are small so that some typical values are also used for describing the thermomechanical properties. The reference temperature is set to  $25^{\circ}\text{C}$  to reflect the climate of Jiufengershan, and the friction angle is set as  $27.4^{\circ}$  (Cecinato and

Zervos 2012). The other parameters used for the Jiufengershan landslide are according to Cecinato and Zervos (2012) and summarized in Table 1.

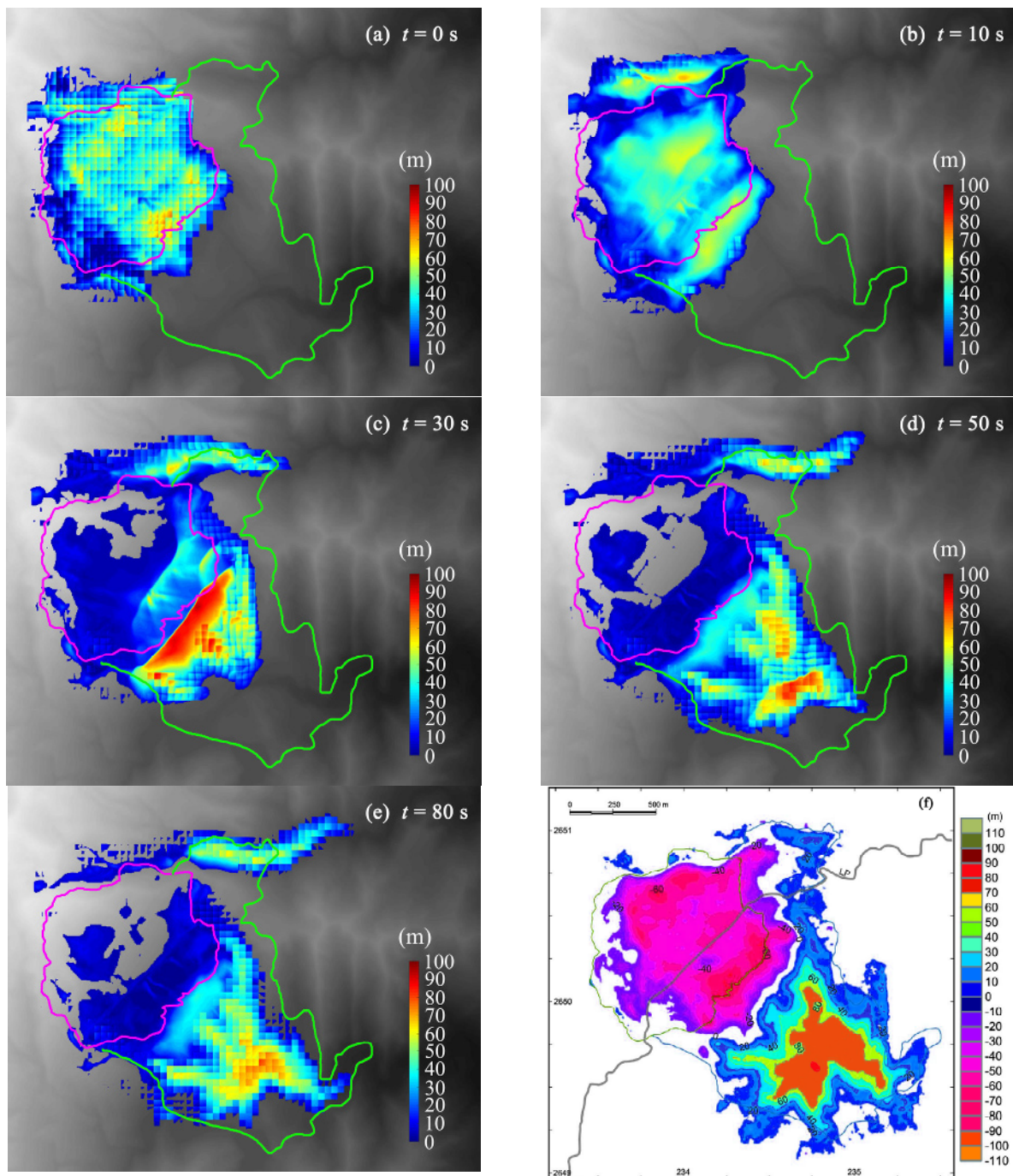
The moving flow depths of the Jiufengershan landslide at five representative times  $t = 0, 10, 30, 50$  and  $80$  s are shown in Figure 11 a-e. It shows



**Figure 10** Map and cross section of the Jiufengershan landslide (modified after Chang et al. 2005). The topographic profiles before and after the slide are indicated in cross section A-A'.

**Table 1** Parameters for Jiufengershan landslide

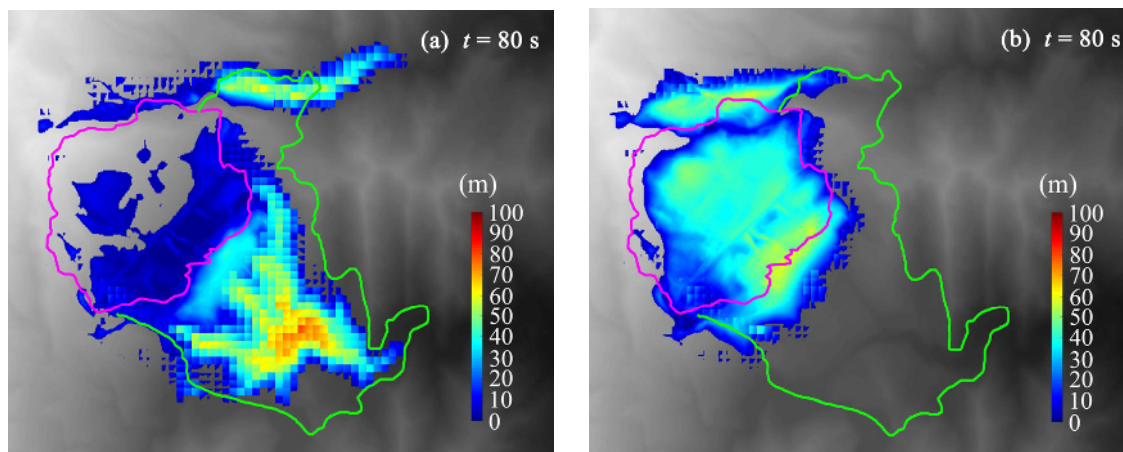
Parameters	Symbol	Value	Units	Parameters	Symbol	Value	Units
Shear zone thickness	$d$	$1.4 \times 10^{-3}$	m	Darcy's permeability coefficient	$k_c$	$10^{-11}$	$\text{m s}^{-1}$
Slope of normal-compression line of soil	$\lambda$	0.17	-	Thermal expansion coefficient of clay	$\alpha_s$	$3 \times 10^{-5}$	$^{\circ}\text{C}^{-1}$
Slope of unloading-reloading line of soil	$\kappa$	$4.5 \times 10^{-2}$	-	Thermal expansion coefficient of water	$\alpha_f$	$2.75 \times 10^{-4}$	$^{\circ}\text{C}^{-1}$
Thermal softening parameter	$\gamma$	$10^{-2}$	-	Solid density	$\rho_s$	2700	$\text{kg m}^{-3}$
Soil void ratio	$e$	0.25	-	Fluid density	$\rho_f$	1000	$\text{kg m}^{-3}$
Compressibility of water	$r_f$	$4.93 \times 10^{-4}$	$\text{MPa}^{-1}$	Solid specific heat	$c_s$	1000	$\text{J kg}^{-1} \text{ } ^{\circ}\text{C}^{-1}$
Soil (drained) Poisson's ratio	$\nu$	0.3	-	Fluid specific heat	$c_f$	4187	$\text{J kg}^{-1} \text{ } ^{\circ}\text{C}^{-1}$
Thermal conductivity of the saturated rock	$k_{\theta}$	0.4	$\text{W m}^{-1} \text{ } ^{\circ}\text{C}^{-1}$				



**Figure 11** The scenarios of Jiufengershan landslide simulation with time at  $t = 0, 10, 30, 50, 80$  s; the background image is hillshade obtained by post-event DEM data. The depletion and accumulation area are contoured by continuous purple and green lines. Figure 9f shows the isopach map of the landslide, and negative and positive values indicate net depletion or accumulation of rock material, respectively (from Chang et al. 2005).

that the mass slid down quickly along two directions after it collapsed. The mass that slide downslope are subsequently folded as they reach the toe of the dip slope along the major slide direction, because of the large monocline. At this stage, the temperature had risen rapidly because of frictional heating, which results in the evolution of

excess pore pressure. The mass was accelerated faster with the gradually decreasing of shear stress, and the maximum value of velocity of sliding mass reached  $53.5 \text{ m s}^{-1}$ . The mass that with high velocity crossed the monocline, and was further transported through a valley incised by the Jiutsaihu creek. Then, as the slope of the terrain



**Figure 12** Comparison of the simulated results between deposit distributions using (a) presented model and (b) Coulomb model at  $t = 80$  s; the background image is obtained by post-event satellite imagery. The depletion and accumulation area are contoured by continuous purple and green lines.

**Table 2** Comparison of two model results with that from some existed literatures

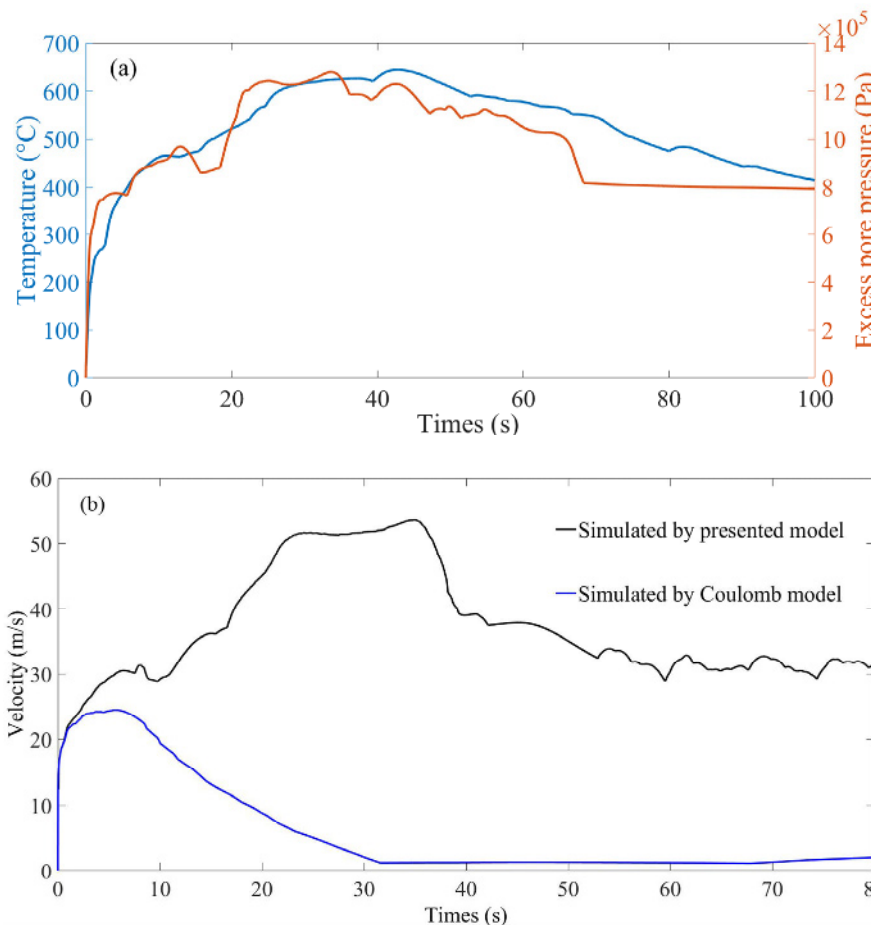
Calculated result	Presented model	Coulomb model	Literature
Initial volume	$3.5 \times 10^7 \text{ m}^3$	$3.5 \times 10^7 \text{ m}^3$	$5 \times 10^7 \text{ m}^3$ (Wang et al. 2003); $4.2 \times 10^7 \text{ m}^3$ (Chang et al. 2009); $4 \times 10^7 \text{ m}^3$ (Tang et al. 2012)
Maximum velocity	$53.5 \text{ m s}^{-1}$	$25.9 \text{ m s}^{-1}$	$80 \text{ m s}^{-1}$ (Chang et al. 2005); $49 \text{ m s}^{-1}$ (Tang et al. 2012)
Maximum depth	82.6 m	62.7 m	110 m (Chang et al. 2009)
Impact area	$9.8 \times 10^5 \text{ m}^2$	$6.3 \times 10^5 \text{ m}^2$	$9.25 \times 10^5 \text{ m}^2$ (Wang et al. 2003)

became small, the mass was decelerated. After that, the sliding mass was blocked by neighbouring steep ridges that trends NS direction, and partially filled the Jiutsaihu valley. The simulated average thickness of the deposit is between 60 and 80 m, which agrees with the measured height (Chang et al. 2005, shown in Figure 11 f). The simulated accumulation area also agrees with the filed observation. However, the simulated maximum velocity is larger than the value of about  $49 \text{ m s}^{-1}$  that is obtained by using a reasonable constant friction coefficient of  $\mu = 0.05$  (Tang et al. 2012) and smaller than the value of about  $80 \text{ m s}^{-1}$  that is obtained by using thermo-mechanical model that with a constant block thickness of 50 m (Chang et al. 2005). Considering that a different kinetic mechanism and initial conditions of landslide are applied in presented model, the simulated velocity is acceptable. Moreover, in order to show the effects of the frictional heating and thermal pressurization on landslide run-out, the Coulomb model that does not consider these effects is also used to simulate the Jiufengershan landslide under the same conditions. The numerical result at  $t = 80$  s following simulation by the Coulomb model is shown in Figure 12. Obviously, the sliding distance of the landslide simulated by the Coulomb model is

very small. It can be found that the velocity of sliding mass decreases rapidly because of large shear stress (shown in Figure 13). Comparison between the two models results with the landslide parameters described in literatures is shown in Table 2. It indicates that the presented model could reflect the high mobility of landslide by considering fractional heating and thermal pressurization. Some differences between landslide parameters and that from other literatures are mainly reflected in the maximum depth and velocity of the deposits. Since the value of the landslide volume used in our model is small, it may reduce the effects of the fractional heating and thermal pressurization on landslide run-out, and further on the values of landslide parameters. Nevertheless, the potential of the presented model to simulate an actual case can be proved.

#### 4 Conclusions

In this paper, a numerical model is presented for investigating the high mobility of landslide by considering frictional heating and thermal pressurization. Based on the staggered-grid technology, a coupled computational scheme is



**Figure 13** Simulated results: (a) evolutions of maximum temperature and excess pore pressure vs. time; (b) evolutions of maximum velocity vs. time.

also proposed to solve the model equations. Numerical results indicate that the thermal pressurization mechanism can be enhanced by frictional heating during landslide run-out, further leading to a greater excess pore pressure at the shear zone, which reduces the frictional resistance. Moreover, the velocity profile that within the shear zone could influence the evolution process of temperature and excess pore pressure obviously, and thus need to be further considered. Finally, the applicability of the presented model is proved by simulating the Jiufengershan landslide that occurred in Taiwan. The influenced area and distribution of sliding mass agrees well with filed observation, which indicates that the presented model has a potential to simulate an actual case.

Compared with other models that consider frictional heating and thermal pressurization, the major feature of the presented model is that it could incorporate this mechanism with depth-averaged model, which makes the effect of this mechanism on landslide run-out could be studied under the condition of deformation. Besides, it also considers the influences of thermal pressurization coefficient that temperature-dependent and velocity profile that within the shear zone on frictional heating and thermal pressurization. However, there are still some aspects needed to be improved for applying the presented model to more landslides. For example, for some huge rock landslide, it may have a slightly or even no deformation at the early stage of sliding, which means

that the effect of thermo-plastic mechanics on landslide run-out may be more obvious.

### Acknowledgments

We thank two anonymous reviewers for their constructive comments. We also do appreciate Dr. M.L. LIN for providing the terrain data of Jiufengershan landslide. This work was supported by the National Natural Science Foundation of China (Grant No. 41790433), NSFC-ICIMOD (Grant No. 41661144041), Key Research and Development Projects of Sichuan Province (2017SZ0041), and CAS "Light of West China" Program.

## References

- Andrews DJ (2002) A fault constitutive relation accounting for thermal pressurization of pore fluid. *Journal of Geophysical Research: Solid Earth* 107(B12). <https://doi.org/10.1029/2002JB001942>
- Abuel-Naga HM, Bergado DT, Bouazza A (2007) Thermally induced volume change and excess pore water pressure of soft Bangkok clay. *Engineering Geology* 89(1): 144-154. <https://doi.org/10.1016/j.enggeo.2006.10.002>
- Ambroso A, Chalons C, Raviart PA (2012) A Godunov-type method for the seven-equation model of compressible two-phase flow. *Computers and Fluids* 54: 67-91. <https://doi.org/10.1016/j.compfluid.2011.10.004>
- Balsara DS (2012) A two-dimensional HLLC Riemann solver for conservation laws: Application to Euler and magnetohydrodynamic flows. *Journal of Computational Physics* 231(22): 7476-7503. <https://doi.org/10.1016/j.jcp.2011.12.025>
- Cleary PW, Campbell CS (1993) Self-lubrication for long runout landslides: Examination by computer simulation. *Journal of Geophysical Research: Solid Earth* 98(B12): 21911-21924. <https://doi.org/10.1029/93JB02380>
- Cui YJ, Sultan N, Delage P (2000) A thermomechanical model for saturated clays. *Canadian Geotechnical Journal* 37(3): 607-620. <https://doi.org/10.1139/t99-111>
- Chang KJ, Taboada A, Lin ML, Chen RF (2005) Analysis of landsliding by earthquake shaking using a block-on-slope thermo-mechanical model: example of Jiufengershan landslide, central Taiwan. *Engineering Geology* 80(1): 151-163. <https://doi.org/10.1016/j.enggeo.2005.04.004>
- Chang KJ, Taboada A, Chan YC (2005) Geological and morphological study of the Jiufengershan landslide triggered by the Chi-Chi Taiwan earthquake. *Geomorphology* 71(3): 293-309. <https://doi.org/10.1016/j.geomorph.2005.02.004>
- Chang KJ, Taboada A (2009) Discrete element simulation of the Jiufengershan rock-and-soil avalanche triggered by the 1999 Chi - Chi earthquake, Taiwan. *Journal of Geophysical Research: Earth Surface* 114(F3). <https://doi.org/10.1029/2008JF001075>
- Cecinato F, Zervos A, Veveakis E (2011) A thermos-mechanical model for the catastrophic collapse of large landslides. *International Journal for Numerical and Analytical Methods in Geomechanics* 35(14): 1507-1535. <https://doi.org/10.1002/nag.963>
- Cecinato F, Zervos A (2012) Influence of thermomechanics in the catastrophic collapse of planar landslides. *Canadian Geotechnical Journal* 49(2): 207-225. <https://doi.org/10.1139/t11-095>
- Dong JJ, Lee WR, Lin ML, et al. (2009) Effects of seismic anisotropy and geological characteristics on the kinematics of the neighboring Jiufengershan and Hungtsaiping landslides during Chi-Chi earthquake. *Tectonophysics* 466(3): 438-457. <https://doi.org/10.1016/j.tecto.2007.11.008>
- De Blasio FV (2011) Landslides in Valles Marineris (Mars): A possible role of basal lubrication by sub-surface ice. *Planetary and Space Science* 59(13): 1384-1392. <https://doi.org/10.1016/j.pss.2011.04.015>
- Domnik B, Pudasaini SP, Katzenbach R, Miller SA (2013) Coupling of full two-dimensional and depth-averaged models for granular flows. *Journal of Non-Newtonian Fluid Mechanics* 201: 56-68. <https://doi.org/10.1016/j.jnnfm.2013.07.005>
- Eismann TH (1979) Mechanisms of large landslides. *Rock Mechanics* 12(1): 15-46. <https://doi.org/10.1007/BF01241087>
- Ferri F, Di Toro G, Hirose T, Shimamoto T (2010) Evidence of thermal pressurization in high-velocity friction experiments on smectite-rich gouges. *Terra Nova* 22(5): 347-353. <https://doi.org/10.1111/j.1365-3121.2010.00955.x>
- Ferri F, Di Toro G, Hirose T, et al. (2011) Low-to high-velocity frictional properties of the clay-rich gouges from the slipping zone of the 1963 Vaiont slide, northern Italy. *Journal of Geophysical Research: Solid Earth* 116(B9). <https://doi.org/10.1029/2011JB008338>
- Fischer JT, Kowalski J, Pudasaini SP (2012) Topographic curvature effects in applied avalanche modeling. *Cold Regions Science and Technology* 74: 21-30. <https://doi.org/10.1016/j.coldregions.2012.01.005>
- Gray JMNT, Tai YC, Noelle S (2003) Shock waves, dead zones and particle-free regions in rapid granular free-surface flows. *Journal of Fluid Mechanics* 491: 161-181. <https://doi.org/10.1017/S0022112003005317>
- Goren L, Aharonov E (2007) Long runout landslides: The role of frictional heating and hydraulic diffusivity. *Geophysical research letters* 34(7). <https://doi.org/10.1029/2006GL028895>
- Goren L, Aharonov E (2009) On the stability of landslides: A thermo-poro-elastic approach. *Earth and Planetary Science Letters* 277(3): 365-372. <https://doi.org/10.1016/j.epsl.2008.11.002>
- Ghabezloo S, Sulem J (2009) Stress dependent thermal pressurization of a fluid-saturated rock. *Rock Mechanics and Rock Engineering* 42(1): 1-24. <https://doi.org/10.1007/s00603-008-0165-z>
- George DL, Iverson RM (2014) A depth-averaged debris-flow model that includes the effects of evolving dilatancy. II. Numerical predictions and experimental tests. *Proceedings of the Royal Society* 470(2170): 20130820. <https://doi.org/10.1098/rspa.2013.0820>
- Habib P (1975) Production of gaseous pore pressure during rock slides. *Rock Mechanics and Rock Engineering* 7(4): 193-197. <https://doi.org/10.1007/BF01246865>
- Hayase T, Humphrey JAC, Greif R (1992) A consistently formulated QUICK scheme for fast and stable convergence using finite-volume iterative calculation procedures. *Journal of Computational Physics* 98(1): 108-118. [https://doi.org/10.1016/0021-9991\(92\)90177-Z](https://doi.org/10.1016/0021-9991(92)90177-Z)
- Huang Y, Dai Z, Zhang W, Chen Z (2011) Visual simulation of landslide fluidized movement based on smoothed particle hydrodynamics. *Natural hazards* 59(3): 1225-1238. <https://doi.org/10.1007/s11069-011-9859-8>
- Huang RQ, Fan XM (2013) The landslide story. *Nature Geoscience* 2103(6): 325-326. <https://doi.org/10.1038/ngeo1806>
- He SM, Liu W, Wang J (2015) Dynamic simulation of landslide based on thermo-poro-elastic approach. *Computers and Geosciences* 75: 24-32. <https://doi.org/10.1016/j.cageo.2014.10.013>
- Hu W, Huang R, McSaveney M, et al. (2018) Mineral changes quantify frictional heating during a large low-friction landslide. *Geology* 46(3): 223-226. <https://doi.org/10.1130/G39662.1>
- Hu W, McSaveney M (2018) A polished and striated pavement formed by a rock avalanche in under 90 s mimics a glacially striated pavement. *Geomorphology* 320: 154-161. <https://doi.org/10.1016/j.geomorph.2018.08.011>
- Iverson RM, Reid ME, Logan M, et al. (2011) Positive feedback and momentum growth during debris-flow entrainment of wet bed sediment. *Nature Geoscience* 4(2): 116-121. <https://doi.org/10.1038/ngeo1040>
- Iverson RM, George DL (2016) Modelling landslide liquefaction, mobility bifurcation and the dynamics of the 2014 Oso disaster. *Geotechnique* 66: 175-187. <https://doi.org/10.1680/jgeot.15.LM.004>
- Johnson CG, Kokelaar BP, Iverson R, et al. (2012) Grain-size segregation and levee formation in geophysical mass flows. *Journal of Geophysical Research: Earth Surface* 117(F1). <https://doi.org/10.1029/2011JF002185>
- Kilgore BD, Blanpied ML, Dieterich J H (1993) Velocity

- dependent friction of granite over a wide range of conditions. *Geophysical Research Letters* 20(10): 903-906. <https://doi.org/10.1029/93GL00368>
- Kuo CY, Tai YC, Chen CC, et al. (2011) The landslide stage of the Hsiaolin catastrophe: Simulation and validation. *Journal of Geophysical Research: Earth Surface* 116(F4). <https://doi.org/10.1029/2010JF001921>
- Leonard BP (1995) Order of accuracy of QUICK and related convection-diffusion schemes. *Applied Mathematical Modelling* 19(11): 640-653. [https://doi.org/10.1016/0307-904X\(95\)00084-W](https://doi.org/10.1016/0307-904X(95)00084-W)
- Laloui L, Cekerevac C, François B (2005) Constitutive modelling of the thermo-plastic behaviour of soils. *Revue européenne de génie civil* 9(5-6): 635-650. <https://doi.org/10.1080/17747120.2005.9692774>
- Liang Q, Borthwick AG (2009) Adaptive quadtree simulation of shallow flows with wet-dry fronts over complex topography. *Computers and Fluids* 38(2): 221-234. <https://doi.org/10.1016/j.compfluid.2008.02.008>
- LeFloch PG, Thanh MD (2011) A Godunov-type method for the shallow water equations with discontinuous topography in the resonant regime. *Journal of Computational Physics* 230(20): 7631-7660. <https://doi.org/10.1016/j.jcp.2011.06.017>
- Mase CW, Smith L (1984) Pore-fluid pressures and frictional heating on a fault surface. *Pure and Applied Geophysics* 122(2-4): 583-607. <https://doi.org/10.1007/BF00874618>
- Miura N, Horpibulsuk S, Nagaraj TS (2001) Engineering behavior of cement stabilized clay at high water content. *Soils and Foundations* 41(5): 33-45. [https://doi.org/10.3208/sandf.41.5\\_33](https://doi.org/10.3208/sandf.41.5_33)
- Mazzanti P, De Blasio FV (2013) The dynamics of subaqueous rock avalanches: the role of dynamic fragmentation. In *Landslide Science and Practice*. Springer Berlin Heidelberg: 35-40. [https://doi.org/10.1007/978-3-642-31427-8\\_4](https://doi.org/10.1007/978-3-642-31427-8_4)
- Noda H, Shimamoto T (2005) Thermal pressurization and slip-weakening distance of a fault: An example of the Hanaore fault, southwest Japan. *Bulletin of the Seismological Society of America* 95(4): 1224-1233. <https://doi.org/10.1785/0120040089>
- Pitman EB, Nichita CC, Patra A, et al. (2003) Computing granular avalanches and landslides. *Physics of Fluids* 15(12): 3638-3646. <https://doi.org/10.1063/1.1614253>
- Pirulli M, Pastor M (2012) Numerical study on the entrainment of bed material into rapid landslides. *Geotechnique* 62(11): 959-972. <https://doi.org/10.1680/geot.10.P.074>
- Pastor M, Stickle MM, Dutto P, et al. (2015) A viscoplastic approach to the behaviour of fluidized geomaterials with application to fast landslides. *Continuum Mechanics and Thermodynamics* 27(1-2): 21-47. <https://doi.org/10.1007/s00161-013-0326-5>
- Rice JR (2006) Heating and weakening of faults during earthquake slip. *Journal of Geophysical Research: Solid Earth* 111(B5). <https://doi.org/10.1029/2005JB004006>
- Rait K, Bowman ET, Lambert C (2012) Dynamic fragmentation of rock clasts under normal compression in sturzstrom. *Geotechnique Letters* 2(3): 167-172. <https://doi.org/10.1680/geolett.12.00038>
- Shreve RL (1968) Leakage and fluidization in air-layer lubricated avalanches. *Geological Society of America Bulletin* 79(5): 653-658. [https://doi.org/10.1130/0016-7606\(1968\)79\[653:LAFIAL\]2.o.CO;2](https://doi.org/10.1130/0016-7606(1968)79[653:LAFIAL]2.o.CO;2)
- Savage SB, Hutter K (1989) The run-out of a finite mass of granular material down a rough incline. *Journal of fluid mechanics* 199: 177-215. <https://doi.org/10.1017/S0022112089000340>
- Sultan N, Delage P, Cui YJ (2002) Temperature effects on the volume change behaviour of Boom clay. *Engineering Geology* 64(2): 135-145. [https://doi.org/10.1016/S0013-7952\(01\)00143-0](https://doi.org/10.1016/S0013-7952(01)00143-0)
- Sulem J, Lazar P, Vardoulakis I (2007) Thermo-poro-mechanical properties of clayey gouge and application to rapid fault shearing. *International Journal for Numerical and Analytical Methods in Geomechanics* 31(3): 523-540. <https://doi.org/10.1002/nag.584>
- Soares-Frazão S, Zech Y (2011) HLLC scheme with novel wave-speed estimators appropriate for two-dimensional shallow-water flow on erodible bed. *International Journal for Numerical Methods in Fluids* 66(8): 1019-1036. <https://doi.org/10.1002/flid.2300>
- Tang ZR, Yuan RM, Hu ZQ, Zheng QQ (2012) 3-D distinct element modelling of sliding process and depositing behaviour in Jiufengershan landslide induced by 1999 Chi-Chi earthquake. *Journal of Engineering Geology* 6: 007. [https://doi.org/10.1004-9665/2012/20\(6\)-0940-15](https://doi.org/10.1004-9665/2012/20(6)-0940-15)
- Tomac I, Gutierrez M (2015) Coupled hydro-thermo-mechanical modeling of hydraulic fracturing in quasi-brittle rocks using DEM. *The Essential Burn Unit Handbook*: 423. <https://doi.org/10.1016/j.jrmge.2016.10.001>
- Voight B, Faust C (1982) Frictional heat and strength loss in some rapid landslides. *Geotechnique* 32(1): 43-54. <https://doi.org/10.1680/geot.1982.32.1.43>
- Vardoulakis I (2000) Catastrophic landslides due to frictional heating of the failure plane. *Mechanics of Cohesive-frictional Materials* 5(6): 443-467. [https://doi.org/10.1002/1099-1484\(200008\)5:6<443::AID-CFM104>3.o.CO;2-W](https://doi.org/10.1002/1099-1484(200008)5:6<443::AID-CFM104>3.o.CO;2-W)
- Vardoulakis I (2002) Dynamic thermo-poro-mechanical analysis of catastrophic landslides. *Geotechnique* 53(3): 157-171. <https://doi.org/10.1680/geot.2002.52.3.157>
- Wang WN, Chigira M, Furuya T (2003) Geological and geomorphological precursors of the Chiu-fen-erh-shan landslide triggered by the Chi-chi earthquake in central Taiwan. *Engineering geology* 69(1): 1-13. [https://doi.org/10.1016/S0013-7952\(02\)00244-2](https://doi.org/10.1016/S0013-7952(02)00244-2)
- Wibberley CA, Shimamoto T (2005) Earthquake slip weakening and asperities explained by thermal pressurization. *Nature* 436(7051): 689-692. <https://doi.org/10.1038/nature03901>